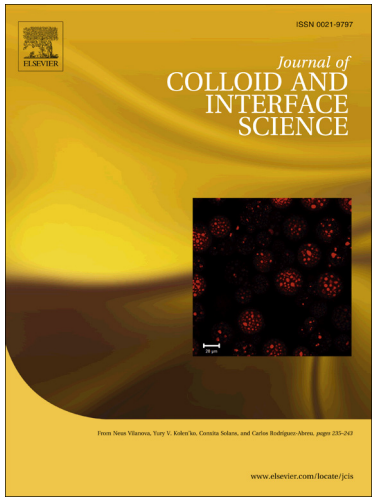

Novel deep eutectic solvent-functionalized carbon nanotubes adsorbent for mercury removal from water

Mohamed Khalid AlOmar, Mohammed Abdulhakim Alsaadi, Taha M. Jassam, Shatirah Akib, Mohd Ali Hashim, Carsten Schwandt

PII: S0021-9797(17)30256-4
DOI: http://dx.doi.org/10.1016/j.jcis.2017.03.014
Reference: YJCIS 22111

To appear in: *Journal of Colloid and Interface Science*

Received Date: 21 October 2016
Revised Date: 18 February 2017
Accepted Date: 2 March 2017

Please cite this article as: M.K. AlOmar, M.A. Alsaadi, T.M. Jassam, S. Akib, M. Ali Hashim, C. Schwandt, Novel deep eutectic solvent-functionalized carbon nanotubes adsorbent for mercury removal from water, *Journal of Colloid and Interface Science* (2017), doi: http://dx.doi.org/10.1016/j.jcis.2017.03.014

Novel deep eutectic solvent-functionalized carbon nanotubes adsorbent for mercury removal from water

Mohamed Khalid AlOmar[a,b], Mohammed Abdulhakim Alsaadi[b,c,d*], Taha M. Jassam[e], Shatirah Akib[g], Mohd Ali Hashim[b,h], Carsten Schwandt[h,i]

[a]Department of Civil Engineering, University of Malaya, Kuala Lumpur 50603, Malaysia

[b]University of Malaya Centre for Ionic Liquids, University Malaya, Kuala Lumpur 50603, Malaysia

[c]Nanotechnology & Catalysis Research Centre (NANOCAT), IPS Building, University of Malaya, 50603 Kuala Lumpur, Malaysia

[d]National Chair Professor of Materials Science and Metallurgy, University of Nizwa, Sultanate of Oman

[d]Civil engineering department, Faculty of engineering, Technology and Built Environment, UCSI University, Kuala Lumpur 56000, Malaysia

[f]School of Energy, Geoscience, Infrastructure and Society (EGIS), Heriot-Watt University Malaysia, 62200, Putrajaya, Malaysia

[g]Department of Chemical Engineering, University of Malaya, Kuala Lumpur 50603, Malaysia

[i]Department of Materials Science and Metallurgy, University of Cambridge, UK

*E-mail: mdsd68j@gmail.com, Tel: +60163630693, Fax: +60 3 7967 5311

Abstract

Due to the interestingly tolerated physicochemical properties of deep eutectic solvents (DESs), they are currently in the process of becoming widely used in many fields of science. Herein, we present a novel Hg^{2+} adsorbent that is based on carbon nanotubes (CNTs) functionalized by DESs. A DES formed from tetra-n-butyl ammonium bromide (TBAB) and glycerol (Gly) was used as a functionalization agent for CNTs. This novel adsorbent was characterized using Raman spectroscopy, Fourier transform infrared (FTIR) spectroscopy, XRD, FESEM, EDX, BET surface area, and Zeta potential. Later, Hg^{2+} adsorption conditions were optimized using response surface methodology (RSM). A pseudo-second order model accurately described the adsorption of Hg^{2+}. The Langmuir and Freundlich isotherms models described the absorption of Hg^{2+} on the novel adsorbent with acceptable accuracy. The maximum adsorption capacity was found to be 177.76 mg/g.

Keywords: Deep eutectic solvents, carbon nanotubes, functionalization, mercury, adsorption

1. Introduction

It is well known that mercury (Hg) is one of the most toxic elements in nature. Hg usually exists in seawater, fresh water, and in soil [1]. In addition, Hg is a waste product associated with many industries, including production of chlor-alkali, fossil fuels, various switches and wiring devices, measuring and control devices, lighting, and dental work [2]. According to the World Health Organization (WHO), the maximum allowable concentration of Hg in water is 1 µg/l. This value is due to its extremely hazardous effects even at low concentrations [3].

Many conventional techniques have been utilized to reduce Hg concentrations in water, including solvent extraction, precipitation, ion-exchange, reverse osmosis, membrane separation, coagulation, and photoreduction [4]. However, most of these methods have drawbacks such as high energy requirements or their association with large quantities of environmentally hazardous chemicals [5]. As a result, Hg removal from water using the adsorption technique proved to be the most applicable on an industrial scale [6, 7].

Recently, nanoparticles have been introduced as extremely effective adsorbents for many pollutants due to their unique features, small size, catalytic potential, high reactivity, and large surface area [8]. Carbon nanotubes (CNTs) have attracted the most attention in the field of water remediation [9]. However, CNTs have yet to be fully optimized in term of solubility, aggregation, and difficulty in manipulation. On the other hand, CNTs have shown a great affinity for interaction with different compounds, especially after surface functionalization [10-17]. Oxidative functionalization can enhance the surface charge of CNTs, but requires the use of strong acids and environmentally unfavorable chemicals. Consequently, the need for new types

of economical and environmentally friendly functionalization agents is crucial for the development of novel applications [18, 19].

Recently, ionic liquids analogues, i.e., deep eutectic solvents (DESs) have utilized in many different scientific fields. DESs were first introduced by Abbot et al. in 2003 as a cheaper replacement for developed ionic liquids (ILs) [20]. Some researchers consider DESs to be the fourth generation of ILs, even though they are not entirely composed of ionic species [21]. Substantially, DESs can be simply defined as a mixture of two or more compounds that has a melting point lower than that of each individual compound [22]. Regarding environmental safety, DESs have met many of the criteria necessary to be considered environmentally friendly solvents, including availability, biodegradability, recyclability, flammability, and relatively low price compared to other conventional solvents [23]. Due to DESs' physicochemical properties, they been used in a variety of applications [24, 25]. Most recently, DESs have achieved wide-spread use in nanotechnology-related fields, with uses such as media for synthesis of nanoparticles [26-31], electrolytes in nanostructure sensors [32], and electrolytes in nanoparticle deposition [33-41]. Based on these applications, DESs have the potential to be used as economically and environmentally friendly functionalization agents.

In this study, an ammonium-based DES was synthesized using tetra-n-butyl ammonium bromide (TBAB) with glycerol (Gly) as the hydrogen bond donor (HBD). Later, this TBAB based-DES was utilized as a functionalization agent for CNTs, which were then used as an adsorbent agent for Hg^{2+} ions from water samples. In addition, the functionalized CNTs were fully characterized as the novel adsorbent to study the effect of TBAB based-DES on the CNT surface. This characterization includes Raman spectroscopy, XRD diffraction, FTIR, FESEM, EDX, BET surface area, and zeta potential. The optimal removal conditions for Hg^{2+} were

determined using Response surface methodology (RSM). Moreover, kinetics and isotherm studies were also performed at the optimal conditions.

2. Experiments and Methods

2.1 Chemicals and materials

Multi-wall carbon nanotubes with specifications of D×L 6-9 nm × 5 μm >95% (carbon), TBAB, Gly, sulfuric acid (95%-97%), nitric acid (65%), potassium permanganate, sodium hydroxide pellets, and hydrochloric acid (36.5-38%) were all supplied by SIGMA- ALDRICH. A 1,000 mg/L mercury standard solution was supplied by MERCK.

2.2 Functionalization of CNTs

The surface of the pristine CNTs (P-CNTs) was functionalized by oxidation through to different procedures. The first procedure used sonication with $KMnO_4$ for 2 hr at 65 ℃ [42]. The resulting oxidized CNTs are referred to as K-CNTs in this study. The second method involved refluxing P-CNTs with HNO_3 (65%) for 1 hr at 140 ℃, and the resulting acidified CNTs are referred to as N-CNTs in this study.

The DESs were synthesized by mixing TBAB with Gly (HBD) using magnetic stirring at 400 rpm and 80℃, until the DESs became a homogeneous liquid without any precipitate. The details of synthesis, characterization, and molar ratio options are based on our previous study [43]. Next, functionalization with the DESs was performed using sonication with 200 mg of P-CNTs, K-CNTs, and N-CNTs, separately, with 7 ml of DES for 3 hr at 65 °C. The resulting functionalized CNTs will be referred to as PT-CNTs, KT-CNTs, and NT-CNTs, respectively. It should be noted that after each functionalization step, the functionalized CNTs were repeatedly washed and filtered with distilled water, using a vacuum pump and a PTFE 0.45 μm membrane, until the filtrate water pH was neutral.

2.3 Characterization of functionalized CNTs

All adsorbents were characterized using a Renishaw System 2000 Raman Spectrometer to obtain Raman shift spectra. The surface modification and functional groups that resulted from the functionalization processes were studied using Fourier transform infrared (FTIR) spectroscopy via a PerkinElmer® FTIR spectrometer USA with a range of 400-4,000 wave number and four times reputation. The structural phases were analyzed using X-ray powder diffraction (XRD) with a Shimadzu XRD 6000® at a scanning range of 2θ between 10°-80°. Furthermore, the surface charge was measured by conducting zeta potential tests using a Zetasizer (Malvern, UK). For the purpose of measuring the zeta potential, 2.5 mg of each adsorbent was dispersed in 5 ml of deionized water and subjected to sonication for 1 hr before the measurement. A fully Automated Gas Sorption System (micromeritics ASAP2020, TRISTAR II 3020 Kr®, USA) was used to study the selected samples surface area, based on the Brunauer-Emmett-Teller (BET) method by adsorption-desorption of nitrogen gas at -200 °C. A Field-Emission Scanning Electron Microscope (Quanta FEG 450, EDX-OXFORD) Thermo Fisher Scientific® USA was used to obtain high resolution nano-sized images for analysis of the morphology of all selected samples, along with an energy-dispersive X-ray spectrometer (EDX). Mercury ions were detected using ICP with an OES OPTIMA7000DV PerkinElmer® USA.

2.4 Adsorption experiments

A primary screening study was conducted to choose the adsorbent with the highest removal percentage. Samples consisting of 10 mg of each adsorbent (P-CNTs, K-CNTs, N-CNTs, PT-CNTs, KT-CNTs, and NT-CNTs) were applied in batch experiments. An Hg^{2+} stock solution with a concentration of 5 mg/L and pH of 2.2 was prepared using distilled water. A similar screening experiment was repeated at pH 6.0. The experiments were conducted using 50 ml of contaminated water in a 250 ml flask with 10 mg of adsorbent. The flask was agitated using a mechanical system for 30 min at room temperature and an agitation speed of 180 rpm.

An estimation of the regression empirical relationship was conducted to assess the removal percentage (R) of Hg^{2+} and the adsorption capacity (Q) of KT-CNTs, utilizing response surface methodology (RSM) [44, 45]. The central composite design (CCD) was selected using the Design Expert V7.0 software. The effects and interactions of three parameters were investigated in this study, specifically pH (3 to 8), contact time (5 to 55 min), and adsorbent dosage (5 to 20 mg). The experimental design, in terms of the actual parameters, alongside R and Q responses are listed in Table 1S (supported information). The optimization was performed at an initial concentration of 3 mg/L. The agitation speed was fixed at 180 rpm.

The rate of ion transfer from the solute to the adsorbent surface and associated parameters are crucial and can be determined by studying the adsorption kinetics. The efficiency of the adsorption process is indicated by the kinetic rate of the adsorption system and, hence, can determine its potential applications. In this study, the removal conditions obtained from the optimization study were applied in the most usable kinetics models, i.e., pseudo-first order and pseudo-second order models. Eq. 1 and Eq. 2 describe the linear form of these two models, respectively.

$$ln(q_e - q_t) = lnq_e - K_1 t \qquad (1)$$

$$\frac{t}{q_t} = \frac{1}{K_2 q_e^2} + \frac{1}{q_e} t \qquad (2),$$

where k_1 and q_e are the slope and intercept calculated by plotting *ln(qe–qt) vs time (t),* respectively, for Eq. 1. q_e is calculated as *1/(slope)* and K_2 is calculated as *(Slope)^2/ intercept.* The slope and the intercept can be determined from a plot of t/q_t *vs t*. The q_e and q_t refer to the adsorption uptake at equilibrium and at time t, respectively, for Eq. 2.

To thoroughly investigate the adsorption mechanism, which can be used for design purposes, it is also essential to define the adsorption isotherm for any novel adsorbents. Herein,

the optimal removal conditions were used with 16 initial Hg^{2+} concentrations (1, 3, 5, 10, 15, 20, 25, 30, 35, 40, 45, 50, 55, 60, 65, and 70 mg/L). The Langmuir and Freundlich isotherm models were used to describe the adsorption of Hg^{2+} on the novel adsorbent. Eq. 3 and Eq. 4 represent the linearized form of the Langmuir and Freundlich models [46-48], respectively.

$$\frac{C_e}{q_e} = \frac{1}{K_a Q_m} + \left(\frac{1}{Q_m}\right) * C_e \quad (3)$$

$$\ln q_e = \ln K_F + \frac{1}{n} \ln C_e \quad (4),$$

where *Ce* is the initial equilibrium concentration, and q_e is the amount of Hg^{2+} absorbed on the surface of the adsorbent. K_a and Q_m are the adsorption equilibrium constant and the maximum adsorption capacity, respectively. In addition, q_e is the uptake of adsorbent. K_F and n are the isotherm constants for the Freundlich isotherm model.

The desorption and regeneration study was achieved by drying KT-CNTs overnight at 100 ˚C, which was primarily used to remove Hg^{2+} with initial concentration of 3 mg/L under the equilibrium optimal removal conditions. Subsequently, different pH solutions were used to desorb Hg^{2+} from KT-CNTs by adding 6 mg of the dried KT-CNT to 50 ml of each solution and shaken at 180 rpm. During the desorption experiment, the concentration was measured at different time intervals. Eq. 5 calculated the Hg^{2+} desorption percentage (D%) [49].

$$D\% = q_D / q_E \times 100\% \quad (5),$$

where *D%* is the desorption of Hg^{2+}, and q_D and q_E are referring to the amount of Hg^{2+} desorption with respect to time and the amount of adsorption at equilibrium, respectively.

3. Results and discussion

The screening studies showed that the KT-CNTs recorded the highest removal compared to other tested adsorbents. The significant effect of TBAB-based DESs on the removal percentage can be seen at both pH 2.2 and pH 6.0. Figure 1 illustrates the screening studies for the adsorption of Hg^{2+}.

For carbon-based materials, Raman spectroscopy is considered to be an essential characterization due its ability to indicate the degree of functionalization by comparing the intensity of the D band (I_D) to that of the G band (I_G) [50]. The I_D/I_G ratio was 1.11, 1.16, and 1.175 for P-CNTs, K-CNTs, and KT-CNTs, respectively. This increase demonstrates the high level of covalent functionalization on the surface of the KT-CNTs through the addition of carboxylic functional groups or other sp3 groups. Furthermore, the third characteristic band known to indicate a carbon-based nanostructure is D′, which appeared as a weak shoulder of the G-band at higher frequencies and can be considered a double resonance feature originating from disorder and defects. It is worth mentioning that the D′ band is undetectable in pure graphite; however, it can be observed in intercalated graphite and MWCNTs [51]. On the other hand, the functionalization with $KMnO_4$ resulted in the presence of MnO_2, which was confirmed by the two peaks at around 575 and 650 cm^{-1} in the K-CNTs spectrum [49, 52]. Next, the additional functional groups that resulted from the functionalization with TBAB-DES reduced the intensity of these peaks and appeared as a small hump. Figure 2 shows the main Raman peaks. Subsequently, FTIR analysis shows that functionalization with TBAB-based DESs results in formation of new functional groups. The N-H stretch is present at wavenumber 3172 cm^{-1} in the KT-CNT spectrum [53]. The presence of O-H is obvious in K-CNTs at 3478 cm^{-1}, however, this peak disappeared after application of DESs as a functionalization agent, which caused some reduction to the surface. In addition, the presence of C-Br^- bonds can be observed in the range of

550 and 650 cm^{-1} for KT-CNTs. The presence of new chemical groups after functionalization with DES provides proof of modification and the creation of various adsorption sites, and increases the adsorption capacity for Hg^{2+}. Figure 3 shows the FTIR spectra for P-CNTs, K-CNTs, and KT-CNTs. The XRD results displayed a typical spectrum of P-CNTs, where (002) and (001), representing the hexagonal graphite structure and the concentric cylinder structure, respectively, are located at 2θ around 26° and 42°, respectively, in the P-CNTs patterns [54]. Figure 4 shows the XRD patterns of P-CNTs, K-CNTs, and KT-CNTs. After functionalization by $KMnO_4$, the peaks almost completely disappeared, which indicates that the deposition of MnO_2 destroys the hexagonal graphite structure of the CNTs by conforming the CNTs into a non-stoichiometric, amorphous shape [55]. The presence of MnO_2 was identified by the two peaks at 2θ around 38° and 65° in the K-CNTs pattern, which can be indexed as (20 l/11 l) and (02 l/31 l), respectively [49]. In the sequential functionalization step, the TBAB-based DES decreased the intensity of these peaks and the main peaks of CNTs were no longer present. This indicates the presence of more sp3 functional groups. Figure 5 shows the FESEM images for P-CNTs, K-CNTs, and KT-CNTs. The presence of MnO_2 and, furthermore, the TBAB-based DESs, are barely observable in the FESEM images, indicating that the MnO_2 was embedded inside the CNTs. Furthermore, an EDX study for KT-CNTs after Hg^{2+} sorption was performed. Figure 1S shows the EDX spectrum of KT-CNTs after adsorption. Also, traceable amounts of Hg^{2+}, Br^-, O, and N were seen in the EDX spectrum.

The zeta potential is the electrical potential between the bulk fluid and the surface across the dielectrical layer attached to the suspended particles in a solution. This potential is a source of balancing electrostatic force that keeps the micro or nano particles stable in suspension or emulation. The absolute zeta potential was found to be 5.5, 45.81, and 59.7 for P-CNTs, K-

CNTs, and KT-CNTs, respectively. Functionalization with $KMnO_4$ resulted in the addition of new oxygen functional groups in form of carbonyl groups and aliphatic carboxylic acids. These functional groups increased the hydrophilicity of the surface, which resulted in increasing surface electronegativity, which plays an important role in the adsorption mechanism [56, 57]. The enhancement in the surface charge also comes from the formation of electronegative active sites, which were generated from the new functional groups and formed by using DESs as a functionalization agent, which significantly increased the zeta potential. It's worth mentioning that there are many factors affecting zeta potential measurements, including particle surface charges, pH, conductivity, ion concentration, and temperature [58]. On the other hand, the effect of TBAB-based DES functionalization on the BET surface area was significant at 123.54, 158.93, and 204.525 m^2/g for P-CNTs, K-CNTs, and KT-CNTs, respectively. In addition, K-CNTs demonstrate a significant reduction in the pore volume to 0.45 cm^3/g as compared to pore volume with P-CNTs at 0.62 cm^3/g. Subsequently, the pore size diameters increased significantly after each functionalization step and were measured at 20.49, 114.12, and 124.8702 Å for P-CNTs, K-CNTs, and KT-CNTs, respectively.

The results obtained from the optimization study for both responses are listed in Table 1S. The highest R was measured at 96.3% under conditions of pH 5.5, contact time 55 min, and adsorbent dosage of 20 mg, and the highest Q was 16.44 mg/g at pH 5.5, contact time 30 min, and adsorbent dosage of 5 mg. The analysis of variance (ANOVA) of R and Q responses implies that both models are significant. Table 2S and Table 3S list the P-values, F- values, and the square mean for both R and Q, respectively. The chance that a "Model F-Value" this large could occur due to noise for both responses is only 0.01% and 1.1%, respectively. These models can be used to successfully navigate the design space and are represented by the following formulas for

regression, Eq. 6 and Eq. 7. The correlation coefficient, R^2, was 0.9491 and 0.9978 for both R and Q, respectively.

$$Hg^{2+}removal\ \%\ (R) = 98.04 + 17.08A + 3.33B + 1.62C - 1.93AB + 0.49AC - 0.55BC - 19.04A^2 - 0.061B^2 - 2.22C^2 \quad (6)$$

$$KT - CNTs\ adsorption\ capacity\ (Q) = 26.16 + 12.65A + 1.11B - 22.64C + 0.63AB - 7.66AC - 0.92BC - 21.45A^2 + 12.69C^2 - 0.56ABC + 12.18A^2C \quad (7),$$

where A, B, and C represent pH, contact time, and adsorbent dosage, respectively.

The relationship between the theoretical values and experimental values is demonstrated in Figure 2S (a and b) for R and Q, respectively. Since the theoretical values predicted by the models developed in this study were quite close to the experimental values, it can be concluded that both models have successfully achieved correlation between the process variables.

Table 1 lists the restrictions developed to control the optimization solutions of the CCD software. The optimal removal conditions were found to be pH 6.4, an adsorbent dosage around 6.0 mg, and a contact time of 45 min. It is well known that the dominant Hg species at pH between 5-8 are Hg^{2+} and $Hg(OH)_2$. The surface charge of the adsorbent also increased inversely with relation to pH, which reduces the H^+ competition with Hg species. Herein, Figure 6 shows the effect of pH on R by fixing the adsorbent dosage to the optimal dose. At the optimum adsorbent dosage, the R increased gradually until it reached the optimal pH of around 6.4, and then remained constant. Meanwhile, the contact time also has a significant effect on R. Conversely, at a maximum adsorbent dosage of 20 mg, the effect of contact time is almost negligible, while the solution pH has a significant effect on the removal of Hg^{2+}. This may be due to the increase in the number of active sites with increased amounts of adsorbent, which makes the adsorption faster and, in turn, the effect of pH more obvious. Figure 3S shows the

effect of pH on Hg removal by fixing the adsorbent dosage to the maximum. On the other hand, the adsorbent dosage has no significant effect on R, as demonstrated in Figure 4S.

Regarding the Q response, the effect of pH is also obvious, as can be seen in Figure 7. Meanwhile, Q increased with the increase in contact time in an attempt to reach equilibrium. Figure 5S demonstrates the effect of adsorbent dosage on Q, although it is well known that Q increases with decreasing adsorbent dosage.

The optimal removal conditions were used to study the adsorption kinetics and isotherms. Based on the values of the correlation coefficients, R^2 was obtained by fitting the experimental data to the pseudo-first order and pseudo-second order kinetics models. Specifically, Hg^{2+} adsorption on the surface of KT-CNTs followed the pseudo-second order kinetics rate since the R^2 was found to be 0.997. On the other hand, the fitting of the pseudo-first order was very poor. Table 2 lists the R^2 and the constants coefficients for each model. These findings agree with previous research on CNTs-based adsorbents [59, 60]. Figure 8 plots the experimental data according to the linearized pseudo-second order model.

MWCNTs and their modified allotropes have a heterogeneous surface. Therefore, the system probably follows multiple mechanisms of adsorption and surface reaction [61, 62].

The functional groups with high electronegativity present on the surface of MWCNTs, such as oxygen-containing groups or C-Br^- bonds, could form complexation with Hg^{2+} ions. Ion exchange processes could also take place with surface-attached H^+ as well. That means, we are in front of two possible probabilities of two different surface reaction reactions, either complexation or proton exchange [49]. On the other hand, OH^- ions in the solution play positive role in consuming H^+, which is why there is enhanced adsorption with the increase of pH to certain point (in our case pH 6.4). However, a further increase in pH leads to an excess amount

of OH^-, which forms complexations with Hg in the solution and reduces the rate of adsorption on the surface [61]. The mechanism that we expect is illustrated in Eq. 8, 9, and 10.

$$2R–OH+Hg^{2+}\rightarrow R–O–Hg–O–R+2H^{+} \quad (8)$$

$$R–COOH-+\ Hg^{2+}\rightarrow R–COOH\text{-}Hg^{+} \quad (9)$$

$$2Hg^{2+}+3OH^{-}\rightarrow Hg(OH)2+Hg(OH)^{+} \quad (10)$$

For the isotherm study, both the Langmuir and Freundlich isotherms models were found to be a fair fit to the experimental data. This behavior can be observed at low concentrations, where there is no contradiction between the two models. It is common in adsorption studies, as stated in many publications listed in Table 3, to have this kind of duality. However, the behavior of the adsorbate-adsorbent system at high concentrations deviates from the ideal gas model. Although the principle assumptions for Langmuir is monolayer-based and Freundlich is multilayer-based, both models can fit with the same set of data at low concentrations and high adsorption capacity for the adsorbent. Herein, the Freundlich isotherm model exhibited more conformity regarding the correlation coefficient, R^2. Table 3 lists the values of R^2 and the isotherm constants for both the Langmuir and Freundlich isotherms models. The suitability of Freundlich model suggests that the adsorption system is heterogeneous by which the adsorption process takes place onto the adsorbent surface which contains different actives sites with various affinities to Hg^{2+} ions and it gives consideration for the roughness of the surface as well as the multilayer approach. To reference the n value ($1<n>10$), the adsorptive behavior is dominated as a physisorption process and indicates the favorability of the Hg^{2+} adsorption on KT-CNTs [63]. Based on these results, the adsorption of Hg^{2+} occurs on a heterogeneous surface with interactions between the adsorbed molecules with a non-uniform distribution of heat of sorption over the surface [64]. Furthermore, some monolayer coverage of Hg^{2+} ions on the surface of the KT-CNTs may be formed according

to the Langmuir fitting data [46]. Figure 9 and Figure 10 plot the linearized adsorption isotherm of KT-CNTs for both the Langmuir and Freundlich equations, respectively.

The recyclability of an adsorbent is essential for practical applications. The simplicity of desorbing metal ions for many cycles of feasible reusability is one of the most important characteristics of a potential industrial adsorbent. The D% was only 10% at pH 5.0 after 3 hr and exceeds 80% at pH 3.0 after 3 hr. The D% was effective at pH $\leq$ 3.0 as seen in Figure 11. The rate of desorption increases with the decrease of pH as demonstrated in Figure 11, where the slope of the curve before equilibrium starts with very low value at pH 4.0 and increases alongside the pH increase until it reaches the highest value at pH 1.3, almost vertical, when the spontaneous desorption takes place. The system reaches equilibrium at different concentrations and at different pHs, also in different equilibrium times. The fastest and highest desorption was seen at pH 1.3 with an equilibrium close to zero. To confirm the viability of regeneration, the recovered adsorbent from the desorption process was dried and reused multiple times. KT-CNTs were successfully reused five times, although the adsorption capacity decreased after each use until it reached 96 mg/g at round five.

4. Conclusion

The Hg^{2+} ion was successfully removed from an aqueous solution by CNTs functionalized with DESs. The novel adsorbent exhibited great potential for Hg^{2+} removal, where the maximum adsorption capacity was found to be 177.76 mg/g, which lies in the highest range compared to the published data. The optimal removal conditions were found to be at pH 6.4, adsorbent dosage of 6.0 mg, and contact time of 45 min. A TBAB-based DESs was synthesized and was a sufficient functionalization agent for CNTs. The effect of TBAB-DES on the surface of CNTs and the enhancement was proved by investigation using Raman spectroscopy, FTIR, XED, Zeta potential, EDX, FESEM, and BET. The characterization showed that using a TBAB-based DES

for functionalization resulted in significantly increasing the surface area of CNTs from 123.54 m^2/g to 204.525 m^2/g. In addition, the presence of new functional groups was detected by FTIR. The functionalized carbon nanomaterials were proven to be sufficient adsorbents for various contaminants, especially Hg^{2+}. With help of DESs, we managed to replace hazardous chemicals in the process of functionalization. These two findings can be a platform for future research and industrial implementation.

5. Acknowledgments

The authors express their thanks to the University of Malaya UMRG (RP017A-13AET) and the National Chair Of Materials Science And Metallurgy, University of Nizwa, Oman for funding this research.

6. References

[1] Mercury Study Report to Congress, in: U.S.E.P. Agency (Ed.) Washington, D.C.: United States Environmental Protection Agency., December 1997.
[2] A. Gupta, S.R. Vidyarthi, N. Sankararamakrishnan, Enhanced sorption of mercury from compact fluorescent bulbs and contaminated water streams using functionalized multiwalled carbon nanotubes, Journal of Hazardous Materials 274 (2014) 132-144.
[3] D. Mohan, V.K. Gupta, S.K. Srivastava, S. Chander, Kinetics of mercury adsorption from wastewater using activated carbon derived from fertilizer waste, Colloids and Surfaces A: Physicochemical and Engineering Aspects 177(2–3) (2001) 169-181.
[4] N.M. Bandaru, N. Reta, H. Dalal, A.V. Ellis, J. Shapter, N.H. Voelcker, Enhanced adsorption of mercury ions on thiol derivatized single wall carbon nanotubes, Journal of Hazardous Materials 261 (2013) 534-541.
[5] F.-S. Zhang, J.O. Nriagu, H. Itoh, Mercury removal from water using activated carbons derived from organic sewage sludge, Water Research 39(2–3) (2005) 389-395.
[6] S. Chiarle, M. Ratto, M. Rovatti, Mercury removal from water by ion exchange resins adsorption, Water Research 34(11) (2000) 2971-2978.
[7] V. Chandra, K.S. Kim, Highly selective adsorption of Hg2+ by a polypyrrole-reduced graphene oxide composite, Chemical Communications 47(13) (2011) 3942-3944.
[8] I. Ali, New Generation Adsorbents for Water Treatment, Chemical Reviews 112(10) (2012) 5073-5091.
[9] R.K. Ibrahim, M. Hayyan, M.A. AlSaadi, A. Hayyan, S. Ibrahim, Environmental application of nanotechnology: air, soil, and water, Environmental Science and Pollution Research 23(14) (2016) 13754-13788.
[10] E.T. Thostenson, Z. Ren, T.-W. Chou, Advances in the science and technology of carbon nanotubes and their composites: a review, Composites Science and Technology 61(13) (2001) 1899-1912.

[11] T. Lin, V. Bajpai, T. Ji, L. Dai, Chemistry of Carbon Nanotubes, Australian Journal of Chemistry 56(7) (2003) 635-651.
[12] A. Hirsch, O. Vostrowsky, Functionalization of Carbon Nanotubes, in: A.D. Schlüter (Ed.), Functional Molecular Nanostructures, Springer Berlin Heidelberg2005, pp. 193-237.
[13] J.E. Fischer, Chemical Doping of Single-Wall Carbon Nanotubes, Accounts of Chemical Research 35(12) (2002) 1079-1086.
[14] Y.-P. Sun, K. Fu, Y. Lin, W. Huang, Functionalized Carbon Nanotubes: Properties and Applications, Accounts of Chemical Research 35(12) (2002) 1096-1104.
[15] R. Andrews, D. Jacques, D. Qian, T. Rantell, Multiwall Carbon Nanotubes: Synthesis and Application, Accounts of Chemical Research 35(12) (2002) 1008-1017.
[16] S. Niyogi, M.A. Hamon, H. Hu, B. Zhao, P. Bhowmik, R. Sen, M.E. Itkis, R.C. Haddon, Chemistry of Single-Walled Carbon Nanotubes, Accounts of Chemical Research 35(12) (2002) 1105-1113.
[17] X. Lu, Z. Chen, Curved Pi-conjugation, aromaticity, and the related chemistry of small fullerenes, Chemical Reviews 105(10) (2005) 3643-3696.
[18] M.T. Martínez, M.A. Callejas, A.M. Benito, M. Cochet, T. Seeger, A. Ansón, J. Schreiber, C. Gordon, C. Marhic, O. Chauvet, W.K. Maser, Modifications of single-wall carbon nanotubes upon oxidative purification treatments, Nanotechnology 14(7) (2003) 691-695.
[19] M. Hayyan, A. Abo-Hamad, M. AlSaadi, M. Hashim, Functionalization of graphene using deep eutectic solvents, Nanoscale Res Lett 10(1) (2015) 1-26.
[20] A.P. Abbott, G. Capper, D.L. Davies, R.K. Rasheed, V. Tambyrajah, Novel solvent properties of choline chloride/urea mixtures, Chemical Communications (1) (2003) 70-71.
[21] M. Cvjetko Bubalo, S. Vidović, I. Radojčić Redovniković, S. Jokić, Green Solvents for Green Technologies, Journal of Chemical Technology & Biotechnology (2015) 1631–1639.
[22] A.P. Abbott, D. Boothby, G. Capper, D.L. Davies, R.K. Rasheed, Deep Eutectic Solvents Formed between Choline Chloride and Carboxylic Acids: Versatile Alternatives to Ionic Liquids, Journal of the American Chemical Society 126(29) (2004) 9142-9147.
[23] Q. Zhang, K. De Oliveira Vigier, S. Royer, F. Jerome, Deep eutectic solvents: syntheses, properties and applications, Chemical Society Reviews 41(21) (2012) 7108-7146.
[24] E.R. Cooper, C.D. Andrews, P.S. Wheatley, P.B. Webb, P. Wormald, R.E. Morris, Ionic liquids and eutectic mixtures as solvent and template in synthesis of zeolite analogues, Nature 430(7003) (2004) 1012-1016.
[25] E. Leroy, P. Decaen, P. Jacquet, G. Coativy, B. Pontoire, A.-L. Reguerre, D. Lourdin, Deep eutectic solvents as functional additives for starch based plastics, Green Chemistry 14(11) (2012) 3063-3066.
[26] M.H. Chakrabarti, N.S.A. Manan, N.P. Brandon, R.C. Maher, F.S. Mjalli, I.M. AlNashef, S.A. Hajimolana, M.A. Hashim, M.A. Hussain, D. Nir, One-pot electrochemical gram-scale synthesis of graphene using deep eutectic solvents and acetonitrile, Chemical Engineering Journal 274 (2015) 213-223.
[27] F. Chen, S. Xie, J. Zhang, R. Liu, Synthesis of spherical Fe3O4 magnetic nanoparticles by co-precipitation in choline chloride/urea deep eutectic solvent, Materials Letters 112 (2013) 177-179.
[28] H. Jia, J. An, X. Guo, C. Su, L. Zhang, H. Zhou, C. Xie, Deep eutectic solvent-assisted growth of gold nanofoams and their excellent catalytic properties, Journal of Molecular Liquids 212 (2015) 763-766.
[29] M. Karimi, S. Hesaraki, M. Alizadeh, A. Kazemzadeh, Synthesis of calcium phosphate nanoparticles in deep-eutectic choline chloride–urea medium: Investigating the role of synthesis temperature on phase characteristics and physical properties, Ceramics International 42(2, Part A) (2016) 2780-2788.
[30] Q.Q. Xiong, J.P. Tu, X. Ge, X.L. Wang, C.D. Gu, One-step synthesis of hematite nanospindles from choline chloride/urea deep eutectic solvent with highly powerful storage versus lithium, Journal of Power Sources 274 (2015) 1-7.

[31] K. Xu, Y. Wang, X. Ding, Y. Huang, N. Li, Q. Wen, Magnetic solid-phase extraction of protein with deep eutectic solvent immobilized magnetic graphene oxide nanoparticles, Talanta 148 (2016) 153-162.
[32] Y. Zheng, L. Ye, L. Yan, Y. Gao, The electrochemical behavior and determination of quercetin in choline chloride/urea deep eutectic solvent electrolyte based on abrasively immobilized multi-wall carbon nanotubes modified electrode, Int. J. Electrochem. Sci 9 (2014) 238-248.
[33] C. Gu, J. Tu, One-Step Fabrication of Nanostructured Ni Film with Lotus Effect from Deep Eutectic Solvent, Langmuir 27(16) (2011) 10132-10140.
[34] Y. You, C. Gu, X. Wang, J. Tu, Electrochemical Synthesis and Characterization of Ni–P Alloy Coatings from Eutectic–Based Ionic Liquid, Journal of The Electrochemical Society 159(11) (2012) D642-D648.
[35] A.P. Abbott, K. El Ttaib, G. Frisch, K.J. McKenzie, K.S. Ryder, Electrodeposition of copper composites from deep eutectic solvents based on choline chloride, Physical Chemistry Chemical Physics 11(21) (2009) 4269-4277.
[36] A. Renjith, A. Roy, V. Lakshminarayanan, In situ fabrication of electrochemically grown mesoporous metallic thin films by anodic dissolution in deep eutectic solvents, Journal of Colloid and Interface Science 426 (2014) 270-279.
[37] A.P. Abbott, K.E. Ttaib, G. Frisch, K.S. Ryder, D. Weston, The electrodeposition of silver composites using deep eutectic solvents, Physical Chemistry Chemical Physics 14(7) (2012) 2443-2449.
[38] X. Guo, S. Wang, J. Gong, J. Guo, L. Peng, W. Ding, Characterization of highly corrosion-resistant nanocrystalline Ni coating electrodeposited on Mg–Nd–Zn–Zr alloy from a eutectic-based ionic liquid, Applied Surface Science 313 (2014) 711-719.
[39] L. Wei, Y.-J. Fan, H.-H. Wang, N. Tian, Z.-Y. Zhou, S.-G. Sun, Electrochemically shape-controlled synthesis in deep eutectic solvents of Pt nanoflowers with enhanced activity for ethanol oxidation, Electrochimica Acta 76 (2012) 468-474.
[40] L. Wei, Z.-Y. Zhou, S.-P. Chen, C.-D. Xu, D. Su, M.E. Schuster, S.-G. Sun, Electrochemically shape-controlled synthesis in deep eutectic solvents: triambic icosahedral platinum nanocrystals with high-index facets and their enhanced catalytic activity, Chemical Communications 49(95) (2013) 11152-11154.
[41] L. Wei, Y.-J. Fan, N. Tian, Z.-Y. Zhou, X.-Q. Zhao, B.-W. Mao, S.-G. Sun, Electrochemically Shape-Controlled Synthesis in Deep Eutectic Solvents—A New Route to Prepare Pt Nanocrystals Enclosed by High-Index Facets with High Catalytic Activity, The Journal of Physical Chemistry C 116(2) (2012) 2040-2044.
[42] M.A. AlSaadi, A. Al Mamun, M.Z. Alam, M.K. Amosa, M.A. Atieh, Removal of Cadmium from Water by CNT–PAC Composite: Effect of Functionalization, Nano 11(01) (2016) 1650011.
[43] M.K. AlOmar, M. Hayyan, M.A. Alsaadi, S. Akib, A. Hayyan, M.A. Hashim, Glycerol-based deep eutectic solvents: Physical properties, Journal of Molecular Liquids 215 (2016) 98-103.
[44] A. Mamun, F. Ma'an, A. Zahirah, M. Yehya, A. Mohammed, M. Alam, S. Muyibi, I. Faris, I. Azni, Optimisation of arsenic adsorption from water by carbon nanofibres grown on powdered activated carbon impregnated with nickel, Journal of Applied Sciences 9(17) (2009) 3180-3183.
[45] A. Fakhri, Investigation of mercury (II) adsorption from aqueous solution onto copper oxide nanoparticles: Optimization using response surface methodology, Process Safety and Environmental Protection 93 (2015) 1-8.
[46] I. Langmuir, THE CONSTITUTION AND FUNDAMENTAL PROPERTIES OF SOLIDS AND LIQUIDS. PART I. SOLIDS, Journal of the American Chemical Society 38(11) (1916) 2221-2295.
[47] A. Al Mamun, Y.M. Ahmed, M.a.F.R. AlKhatib, A.T. Jameel, M.A.H.A.R. AlSaadi, Lead Sorption by Carbon Nanofibers Grown on Powdered Activated Carbon — Kinetics and Equilibrium, Nano 10(02) (2015) 1550017.
[48] H. Freundlich, H.S. Hatfield, Colloid and capillary chemistry, (1926).

[49] M.K. AlOmar, M.A. Alsaadi, M. Hayyan, S. Akib, M. Ibrahim, M.A. Hashim, Allyl triphenyl phosphonium bromide based DES-functionalized carbon nanotubes for the removal of mercury from water, Chemosphere 167 (2017) 44-52.
[50] T.J. Aitchison, M. Ginic-Markovic, J.G. Matisons, G.P. Simon, P.M. Fredericks, Purification, Cutting, and Sidewall Functionalization of Multiwalled Carbon Nanotubes Using Potassium Permanganate Solutions, The Journal of Physical Chemistry C 111(6) (2007) 2440-2446.
[51] C.S. Kumar, Raman spectroscopy for nanomaterials characterization, Springer Science & Business Media2012.
[52] A. Ogata, S. Komaba, R. Baddour-Hadjean, J.P. Pereira-Ramos, N. Kumagai, Doping effects on structure and electrode performance of K-birnessite-type manganese dioxides for rechargeable lithium battery, Electrochimica Acta 53(7) (2008) 3084-3093.
[53] B.C. Smith, Infrared spectral interpretation: a systematic approach, CRC press1998.
[54] D. Zhang, L. Shi, J. Fang, X. Li, K. Dai, Preparation and modification of carbon nanotubes, Materials Letters 59(29-30) (2005) 4044-4047.
[55] S.-G. Wang, W.-X. Gong, X.-W. Liu, Y.-W. Yao, B.-Y. Gao, Q.-Y. Yue, Removal of lead(II) from aqueous solution by adsorption onto manganese oxide-coated carbon nanotubes, Separation and Purification Technology 58(1) (2007) 17-23.
[56] M.K. AlOmar, M.A. Alsaadi, M. Hayyan, S. Akib, R.K. Ibrahim, M.A. Hashim, Lead removal from water by choline chloride based deep eutectic solvents functionalized carbon nanotubes, Journal of Molecular Liquids 222 (2016) 883-894.
[57] M.K. AlOmar, M.A. Alsaadi, M. Hayyan, S. Akib, M.A. Hashim, Functionalization of CNTs surface with phosphonuim based deep eutectic solvents for arsenic removal from water, Applied Surface Science 389 (2016) 216-226.
[58] G.S. Simate, S.E. Iyuke, S. Ndlovu, M. Heydenrych, The heterogeneous coagulation and flocculation of brewery wastewater using carbon nanotubes, Water Research 46(4) (2012) 1185-1197.
[59] J. Gong, J. Feng, J. Liu, Z. Jiang, X. Chen, E. Mijowska, X. Wen, T. Tang, Catalytic carbonization of polypropylene into cup-stacked carbon nanotubes with high performances in adsorption of heavy metallic ions and organic dyes, Chemical Engineering Journal 248(0) (2014) 27-40.
[60] C. Zhang, J. Sui, J. Li, Y. Tang, W. Cai, Efficient removal of heavy metal ions by thiol-functionalized superparamagnetic carbon nanotubes, Chemical Engineering Journal 210(0) (2012) 45-52.
[61] M. Hadavifar, N. Bahramifar, H. Younesi, Q. Li, Adsorption of mercury ions from synthetic and real wastewater aqueous solution by functionalized multi-walled carbon nanotube with both amino and thiolated groups, Chemical Engineering Journal 237 (2014) 217-228.
[62] P.H. Chen, C.-F. Hsu, D.D.-W. Tsai, Y.-M. Lu, W.-J. Huang, Adsorption of mercury from water by modified multi-walled carbon nanotubes: adsorption behaviour and interference resistance by coexisting anions, Environmental Technology 35(15) (2014) 1935-1944.
[63] T.A. Saleh, Isotherm, kinetic, and thermodynamic studies on Hg(II) adsorption from aqueous solution by silica- multiwall carbon nanotubes, Environmental Science and Pollution Research 22(21) (2015) 16721-16731.
[64] M. Ghaedi, A. Hassanzadeh, S.N. Kokhdan, Multiwalled Carbon Nanotubes as Adsorbents for the Kinetic and Equilibrium Study of the Removal of Alizarin Red S and Morin, Journal of Chemical & Engineering Data 56(5) (2011) 2511-2520.

Table 1 Constraints for optimization process based on CCD for Hg^{2+} adsorption

Name	Goal	Lowe limit	Upper limit	Importance
A	is in range	3	8	3
B	is in range	5	55	3
C	is in range	5	20	3
R	maximize	51.98	99.43	5
Q	maximize	1.81	61.51	5

Table 2 Experimental values of constants of adsorption kinetics models

Experimental (q)	Pseudo-first- order			Pseudo-second-order		
	q_e (mg/g)	K_1 (min^1).	R^2	q_e (mg/g)	K_2 (g/mg.min)	R^2
23.928	22.718	-0.00049	0.545	25.976	0.0037	0.997

Table 3 isotherm models parameters and comparison of adsorption capacity of other adsorbents

Adsorption Isotherm Model		Langmuir			Freundlich			Reference
Adsorbent	pH	q_m (mg/g)	K_L (l/mg)	R^2	n	K_f (mg/g)	R^2	
KT-CNTs	6.5	177.76	9.77	0.949	2.695	37.92	0.976	Present work
[a]MWCNTs-SH		84.66	0.31	0.945	0.301	30.92	0.926	[61]
[b]SiO2-CNT	5-6	250	0.14	0.982	1.50	34.80	0.992	[63]
[c]CNT-S	6	151.51	0.3143	0.994	1.835	1.24	0.936	[2]
[d]COOH-MWCNT	4.3	127.6	0.19	0.990	1.17	18.04	0.968	[62]
[e]MPTS-CNTs/$Fe3O_4$	6.5	65.52	0.039	0.992	2.269	7.62	0.984	[60]

[a]sodium 2-mercaptoethanol functionalized CNT, [b]Silica combined with 2 % functionalized CNT, csulfur incorporated MWCNT, dpre-treated MWCNT in acidic KMnO4/H2SO4 solution, [e]Thiol-functionalized multiwall carbon nanotube/magnetite nanocomposites.

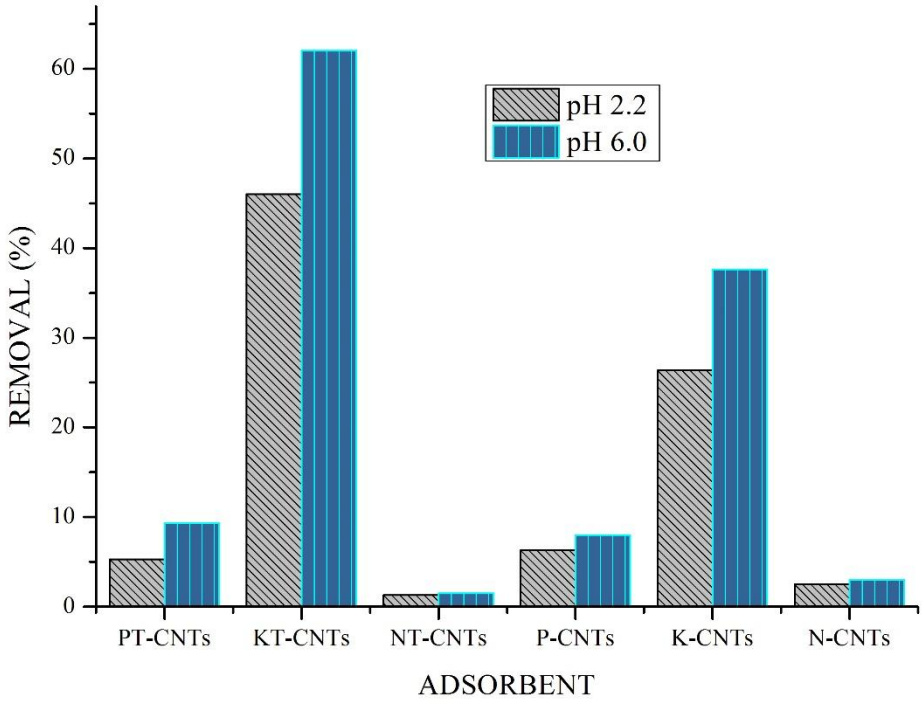

Figure 1 primary screening study for all adsorbents

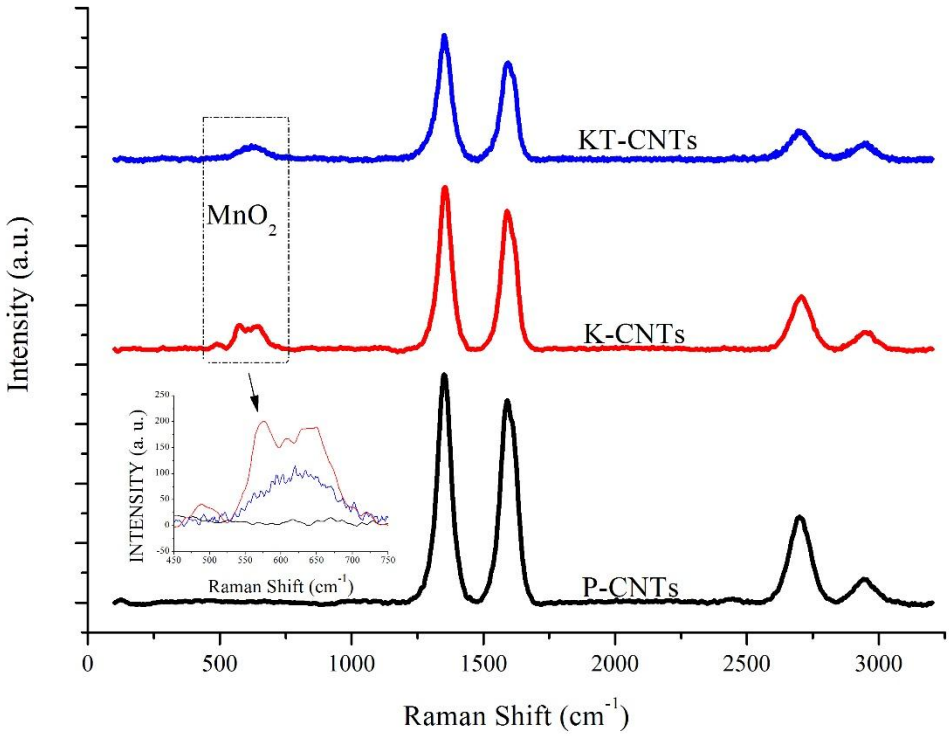

Figure 2 Raman Spectrum of P-CNTs, K-CNTs and KT-CNTs

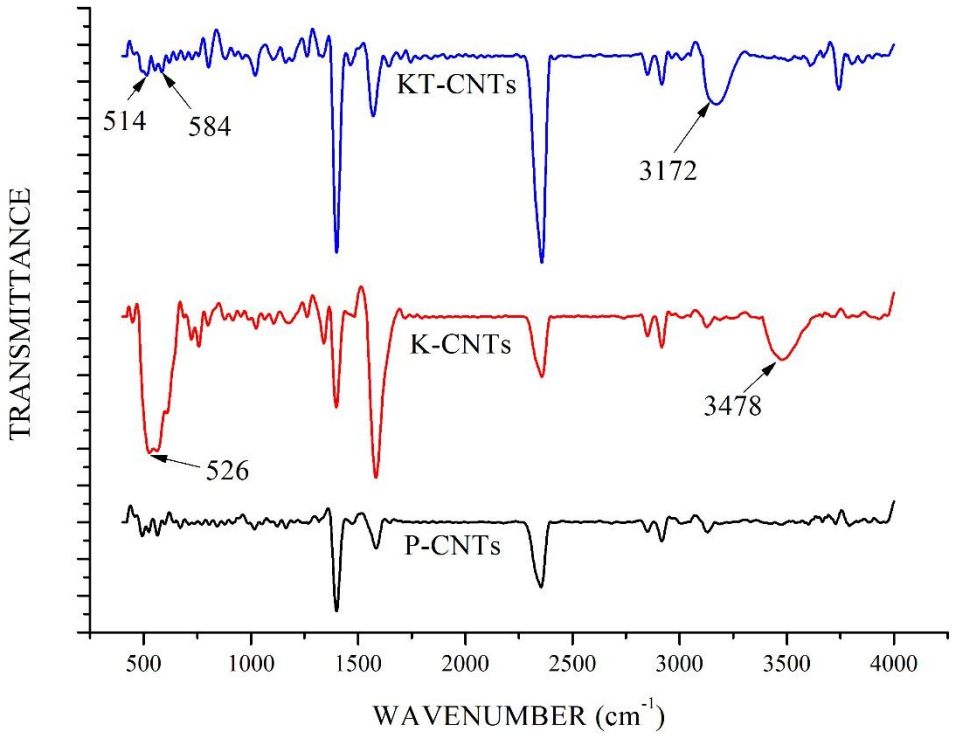

Figure 3 FTIR spectrum for P-CNTs, K-CNTs and KT-CNTs

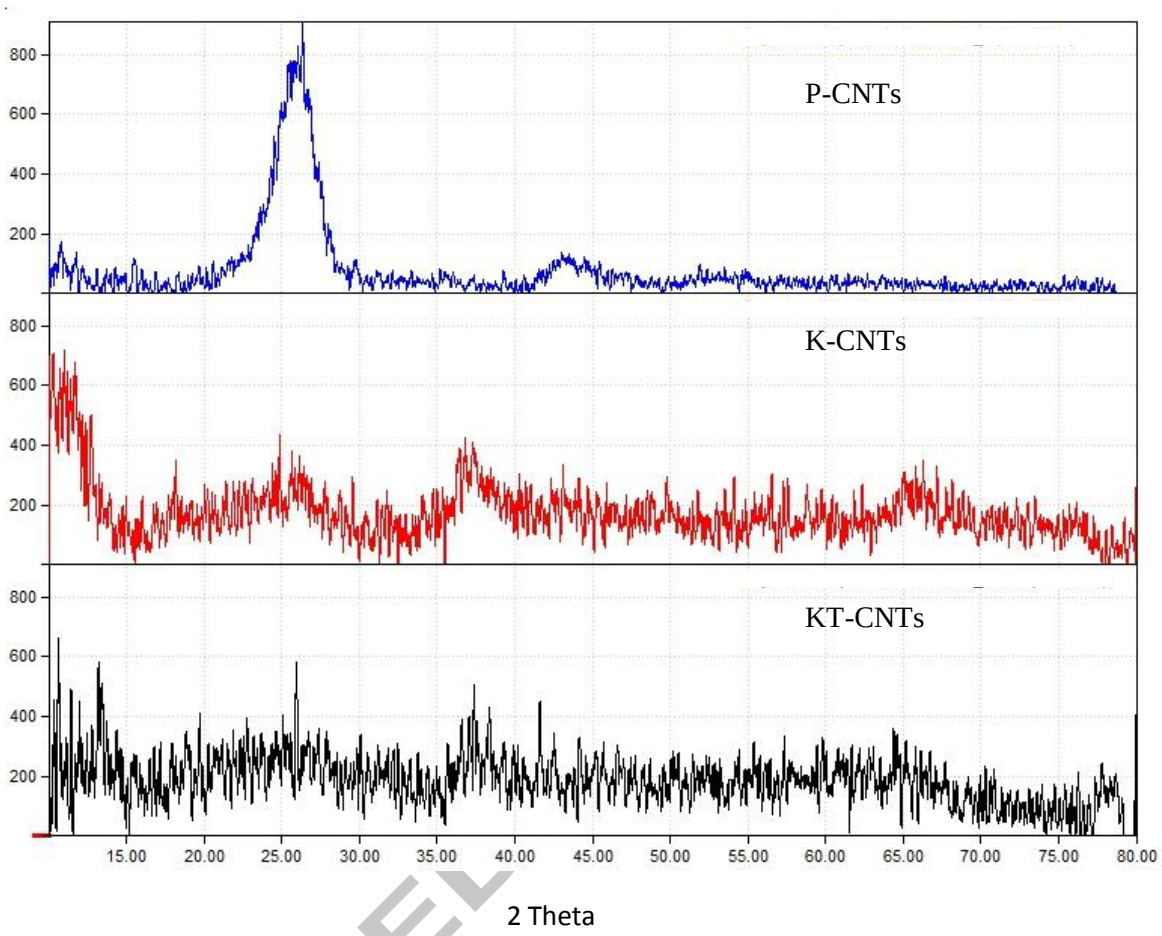

Figure 4 XRD pattern of P-CNTs, K-CNTs, and KT-CNTs

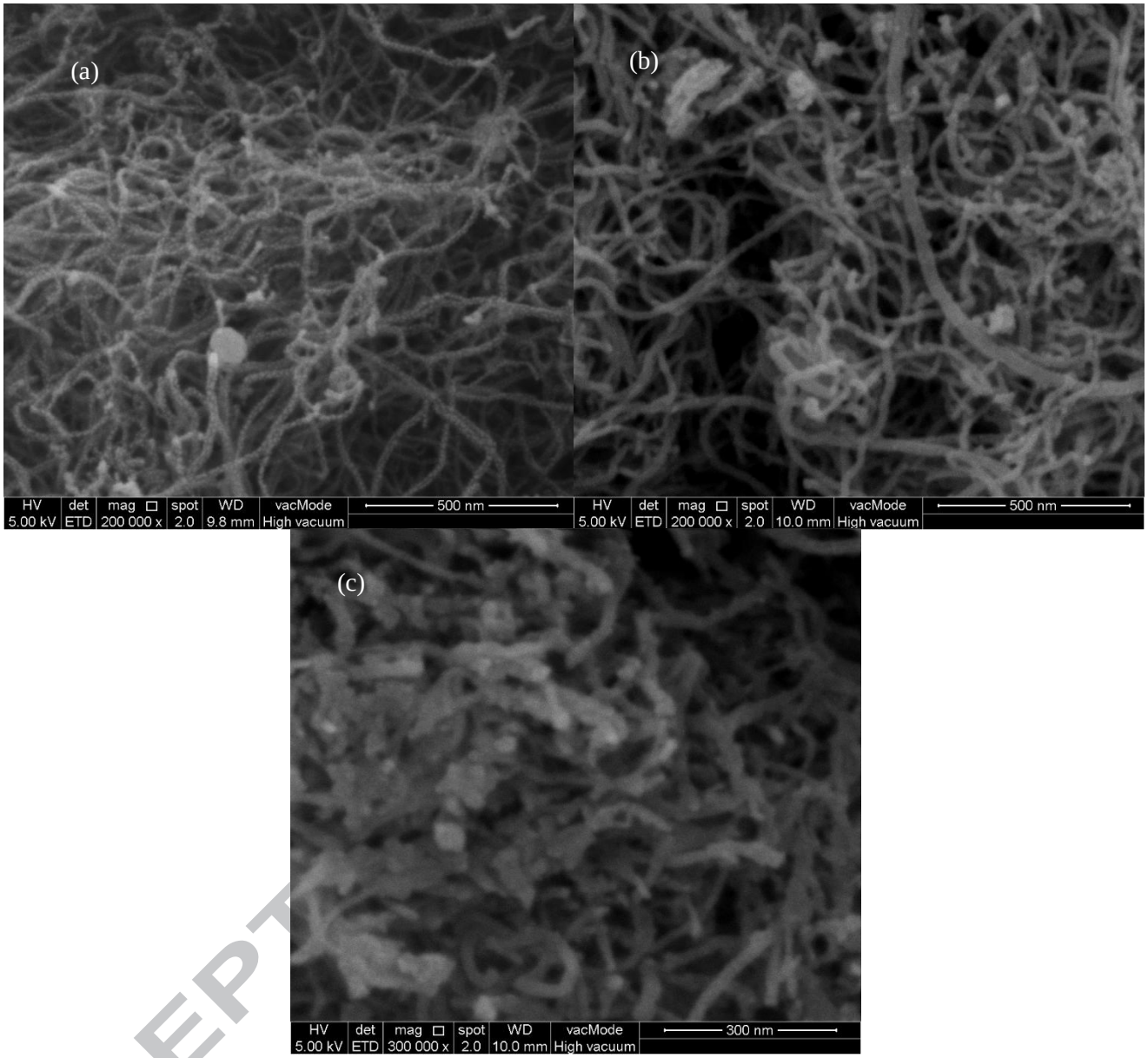

Figure 5 FESEM images for a) P-CNTs, b) K-CNTs and c) KT-CNTs

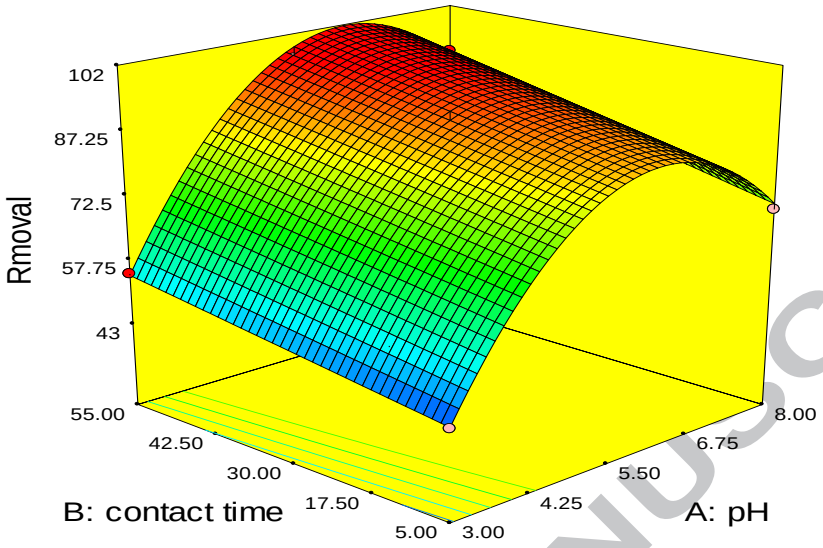

Figure 6 effect of pH and contact time on the R % at the optimum adsorbent dosage

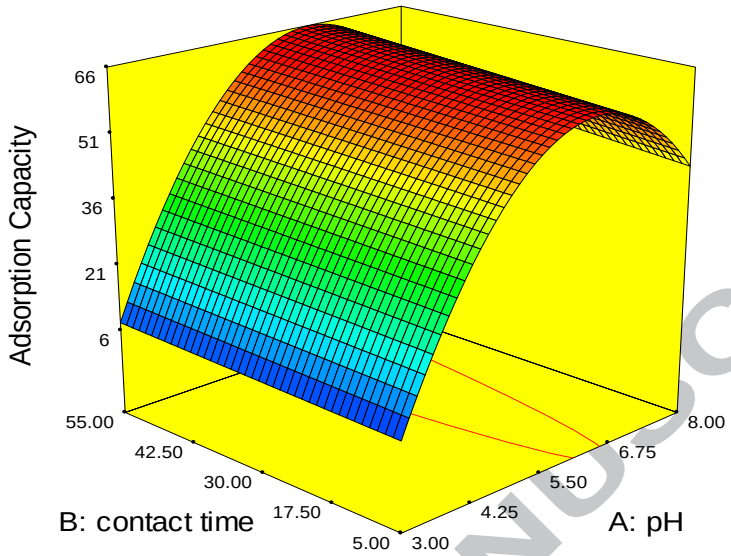

Figure 7 effect of pH and contact time on the adsorption capacity of KT-CNTs

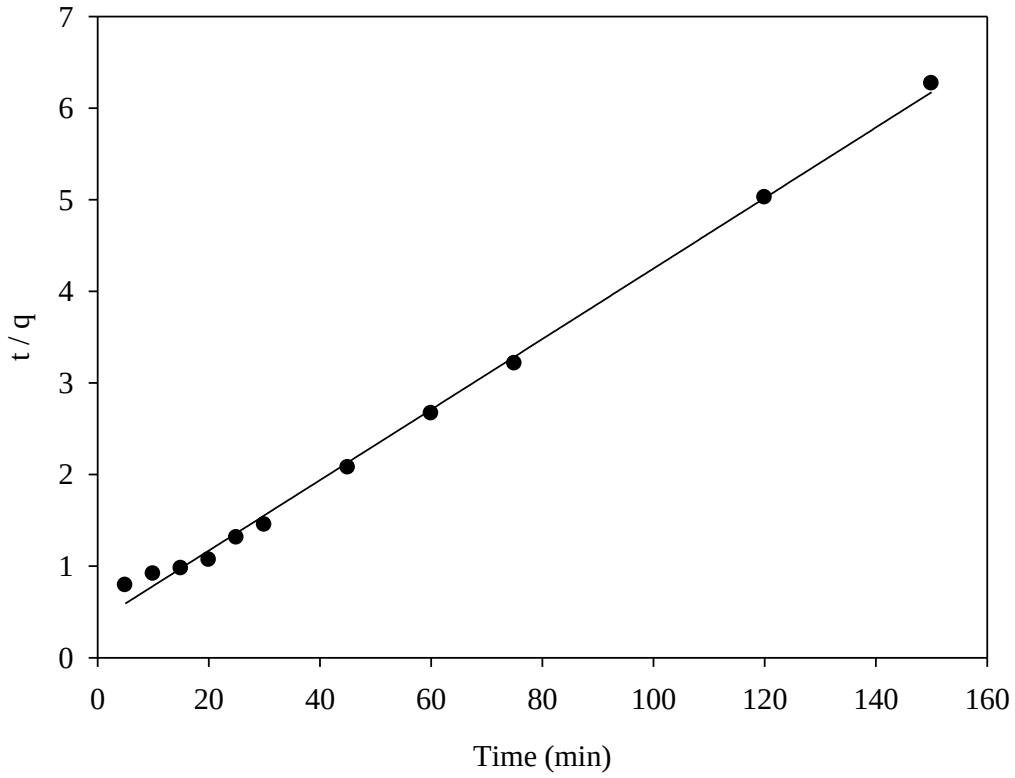

Figure 8 pseudo-second-order adsorption kinetics model

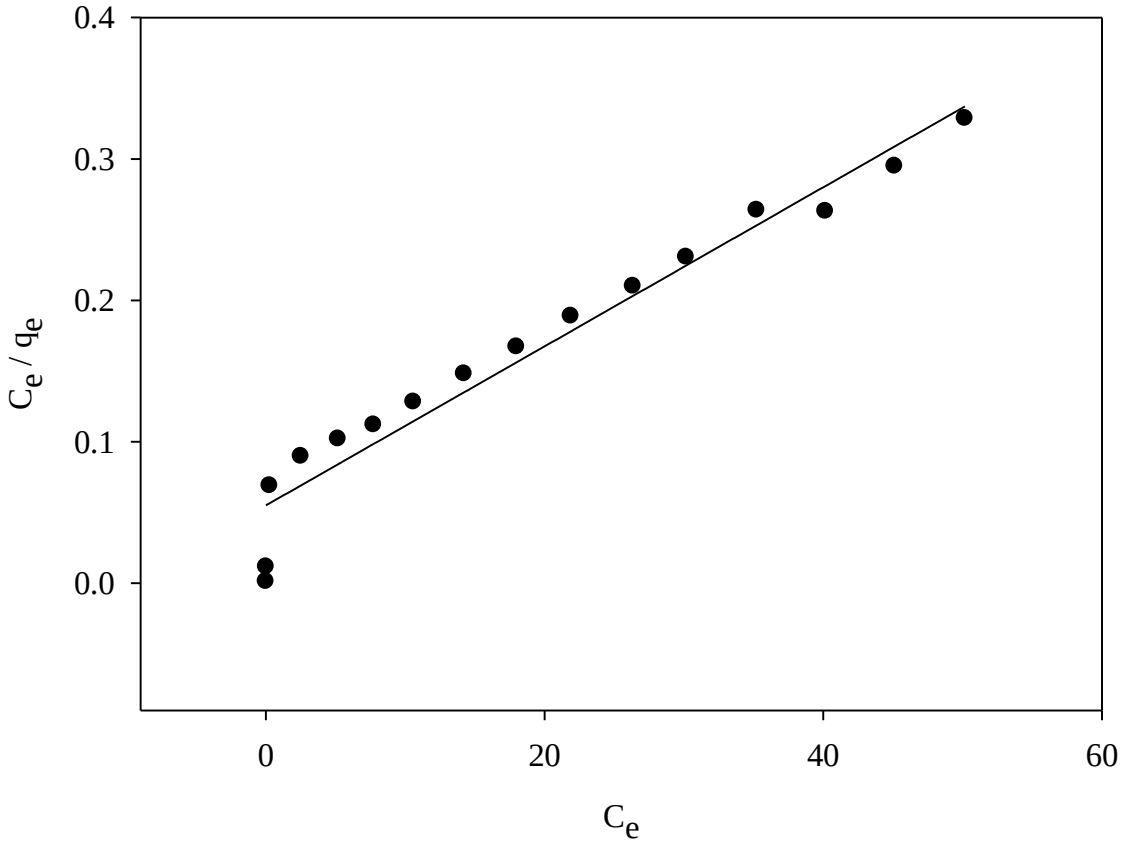

Figure 9 Langmuir adsorption isotherm model

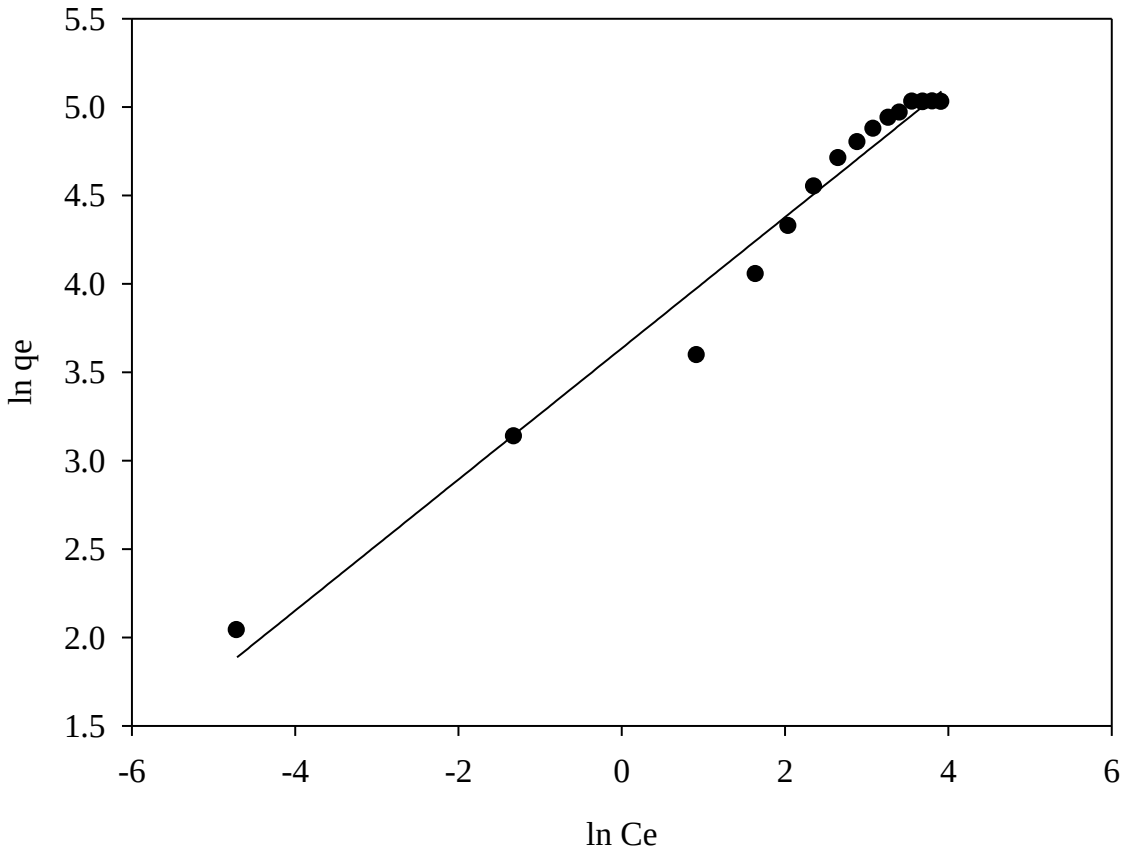

Figure 10 Freundlich adsorption isotherm model

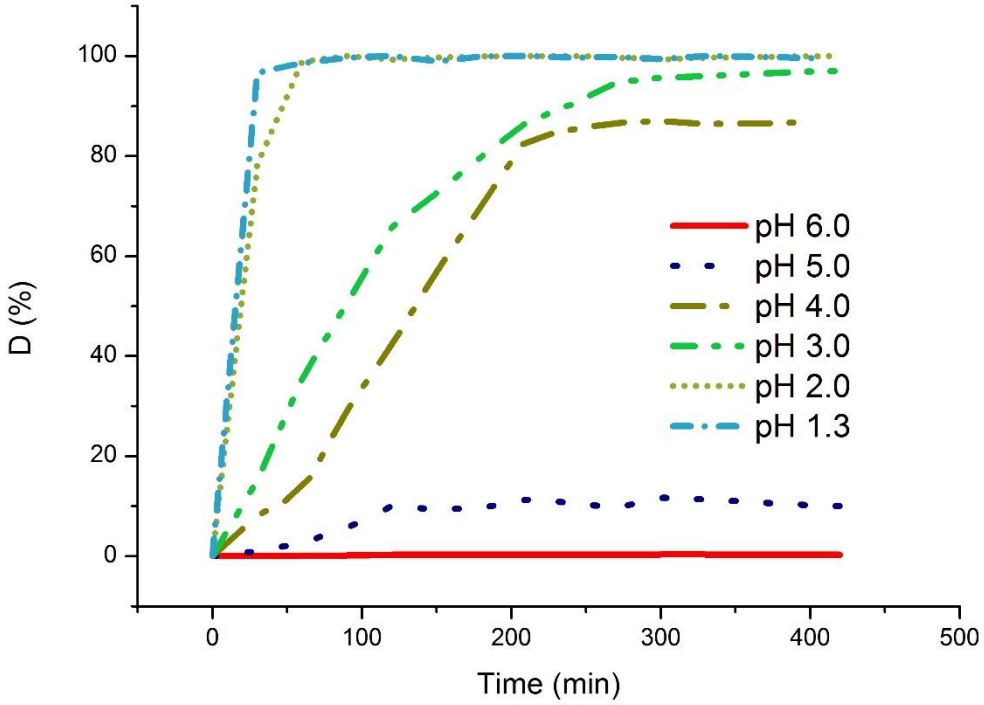

Figure 11 desorption study of Hg^{2+} from KT-CNTs at different pHs

Graphical Abstract